Journal of Applied Electrochemistry (2006) 36:303–308
DOI 10.1007/s10800-005-9073-z

Corrosion behaviour of aluminium metal matrix composites reinforced with TiC processed by pressureless melt infiltration

A. ALBITER[1,*], A. CONTRERAS[1], M. SALAZAR[1] and J.G. GONZALEZ-RODRIGUEZ[2]
[1]*Tecnología de Materiales, Instituto Mexicano del Petróleo, Eje central Lázaro Cárdenas # 152, San Bartolo Atepehuacan, C. P. 07730, México D.F, México*
[2]*UAEM-CIICAP, Av. Universidad 1001, Col. Chamilpa, Cuernavaca, 6225 Morelos, México*
*(*author for correspondence, e-mail: aalbiter@imp.mx)*

Received 10 July 2005; accepted in revised form 9 September 2005

Key words: Al-2024 alloy, composites, corrosion, infiltration, TiC

Abstract

The corrosion resistance of commercial aluminium alloy (2024) and binary Al–Cu_x and Al–Mg_x alloys reinforced with TiC particles using a pressureless infiltration method has been evaluated in 3.5% NaCl solution using potentiodynamic polarization curves and linear polarization resistance measurements. The TiC preforms were sintered at 1250, 1350 and 1450 °C and infiltrated in the range of 900–1200 °C under argon atmosphere. Some specimens were heat treated at 530 °C for 150 min, water quenched and subsequently artificially aged at 190 °C for 12 h in an argon atmosphere and naturally aged at room temperature for 96 h, respectively. The corrosion resistance of the composites was evaluated as a function of the addition of Cu and Mg into the aluminium. In all cases pitting corrosion was observed with or without additions of Cu or Mg, but these elements increased the anodic corrosion current. However, it was found that addition of TiC particles in the composite without heat treatment reduced the anodic current density and the number and size of pits in the Al-2024 alloy. When the heat treatment was applied to the composite, either artificially or naturally aged, the anodic current density of the Al-2024 alloy increased.

1. Introduction

Aluminium-alloy based metal matrix composites have the highest priority in applications where a combination of corrosion resistance, low density and high mechanical performance are required, such as in the automotive and aerospace industry.

The reinforcement of an aluminium matrix, based on the use of TiC particles is interesting because of its good wettability [1, 2] which results in a clean and strong interface [2–4]. While aluminium alloys are the most common matrix used in metal-ceramic composites, it is reported that the addition of TiC, as reinforcement, improves the mechanical properties at room and high temperatures. In particular, the AlCu-alloy/TiC system provides a favourable combination of electrical and mechanical properties. Comparatively, AlMg-alloy/TiC composites are lighter than AlCu-alloy/TiC.

The interface between the matrix and reinforcement plays a crucial role in determining the properties of Metal Matrix Composites (MMCs). Mechanical and physical properties of the MMCs such as strength, stiffness, ductility, toughness, fatigue resistance, creep resistance, thermal expansion coefficient, thermal conductivity and corrosion resistance are dependent on the interfacial behaviour [5]. The main concern is the high corrosion tendency of Al-alloys worsened by the galvanic corrosion between the metallic matrix and more noble fibers or particle reinforcement. Therefore, it is important to study the corrosion behaviour of composites for their application.

The corrosion behaviour of composites reinforced with different ceramics, such as Al_2O_3, SiC and TiC has been studied by Deuis et al. [6] in 3.5 wt.% sodium chloride solution. They found that the corrosion rate increases in the following order: $Al_2O_3 <$ SiC $<$ TiC. The corrosion rates of composites were higher than their matrix alloys when they were immersed in NaCl solutions. This has been attributed to localized attack of the MMC at the matrix interface, resulting in pitting or crevice corrosion. The interfaces were preferred sites for passive film breakdown (pitting initiation sites), that produce voids, resulting in an easier breakdown of the oxide layer [7–9]. Pitting in composites has been observed at the reinforcement matrix interface [10–12]. Factors influencing the corrosion of composites include porosity, precipitation of intermetallic phases within the matrix, high dislocation densities at the particle-matrix

interfaces, the presence of an interfacial reaction product and electrical conductivity of the reinforcements.

Although research has been carried out on the corrosion behaviour of composites, some controversies still exist. The literature on the corrosion behaviour of metal matrix composites [13, 14] has shown that the presence of reinforcement can increase the corrosion susceptibility, depending of the metal-reinforcement combination and the manufacturing process parameters. The use of Al–Cu alloys to fabricate MMCs by liquid metal infiltration can lead to the formation of intermetallics, such as $CuAl_2$, which increase some mechanical properties of the alloy and can act as local anodes or cathodes, inducing a high susceptibility to localized types of corrosion like pitting, intergranular attack, etc. Localized pitting in the vicinity of copper aluminide ($CuAl_2$) precipitates within the 2000 series of aluminium alloys was also observed [15].

The aim of the present work was to investigate the aqueous corrosion behaviour of aluminium metal matrix composites reinforced with TiC particles, produced by the melt infiltration technique.

2. Experimental procedure

2.1. *Samples preparation*

The Al-alloy/TiC composites were produced by pressureless melt infiltration of Al-alloys into TiC preforms. The average size of the reinforcing TiC powder was 1.12 μm. These powders were uniaxially pressed into bars of approximately $6.5 \times 1.0 \times 1.0$ cm in size. After, the green bars were partially sintered in an argon atmosphere at 1250, 1350 and 1450 °C during 90 min, obtaining preforms with 44–48% of porosity. Infiltration was carried out at 1100, 1150 and 1200 °C in an argon atmosphere with a cooling rate of 12–15 °C min^{-1} for the 2024 commercial aluminium alloy. Meanwhile, the binary aluminium alloys were infiltrated at 900 and 1000 °C and the preforms used were sintered at 1250 °C, both in an argon atmosphere. The chemical composition of the 2024 alloy employed was Al–4.23Cu–1.43 Mg–0.55Mn–0.4Fe–0.3Si–0.14Zn (wt.%). In addition, some specimens (Al-2024/TiC) were heat treated at 530 °C for 150 min, water quenched, and subsequently artificially aged at 190°C for 12 h in an argon atmosphere and naturally aged at room temperature for 96 h, respectively.

2.2. *Electrochemical measurements*

Electrochemical experiments were performed using an ACM Instruments potentiostat controlled by a personal computer. The applied potential ranged from ± 1000 mV, referred to the free corrosion potential, E_{corr}, at a scan rate of 1 mV s^{-1}. A saturated calomel electrode and graphite electrode were used as reference and auxiliary electrodes respectively. Before starting the experiments, the E_{corr} value was measured for approximately 30 min, to ensure stability. Corrosion rates were calculated in terms of the corrosion current density, I_{corr}, by using linear polarization resistance (LPR) measurements. These measurements were carried out by polarizing the specimen from +10 to −10 mV with respect to E_{corr}, at a scan rate of 1 mV s^{-1} and calculating the polarization resistance using the Stearn–Geary [16] equation:

$$I_{corr} = \frac{b_a b_c}{2.3(b_a + b_c)} \bullet \frac{1}{R_p} \quad (1)$$

where b_a and b_c are the anodic and cathodic Tafel slopes obtained from the polarization curves. During the experiment, the E_{corr} values were measured using a digital voltmeter, at intervals of 10 min. Thus, the variation of E_{corr} and the polarization resistance, R_p, as a function of time, were recorded. All tests were performed at room temperature (25 °C ±2°C). An aqueous solution of 3.5 (wt.%) NaCl was used as electrolyte and was prepared from analytical grade reagents. The microstructure of the specimens, before and after the experiments, was observed by Scanning Electron Microscopy (XL-30 ESEM Philips).

3. Results and discussion

The microstructural and chemical characterization results are given elsewhere [4, 17]. X-ray diffraction (XRD) studies performed on the as-fabricated materials and heat treated composites indicated the presence of intermetallic phases such as $CuAl_2$, $TiAl_3$, Ti_3AlC, and $AlTi_3$. For both aged conditions, the X-ray diffraction patterns indicated the presence of Al_3Ti and Ti_3AlC phases in addition to Al and TiC. The same phases were detected for specimens either artificially or naturally aged, except the $CuAl_2$ phase, which was dissolved into the matrix when a solution heat treatment was applied. The slow cooling rate after infiltration, led to the formation of phases such as the Ti_3AlC, which is an intermediate compound between the $TiAl_3$ and TiC. XRD showed that Mg forms a solid solution with the aluminium lattice and no reaction phase was detected, since magnesium does not form stable carbides [2, 4, 5, 18]. The presence of these precipitates, especially those containg copper, is detrimental to the corrosion behaviour, since the Cu–Al galvanic coupling (being Cu the cathode) will produce sites for localized type of corrosion such as pitting. Figure 1 shows typical micrographs of samples, sintered at 1250 °C and infiltrated at 1000 °C. This figure shows the microstructure of the as-infiltrated and Al alloy–TiC composites. The dark phase is the aluminium matrix and the white bright phase is related to the TiC grains. The SEM micrographs show that the earlier porous network was occupied by the aluminium alloys, forming a continuous interconnected metal matrix.

Figures 2a–c show the effect of infiltration temperature on the anodic current density for the composites sintered at 1250, 1350 and 1450 °C, respectively. For the specimens sintered at 1250 °C (Figure 2a), the lowest anodic current density was obtained due at the lowest infiltrating temperature (1100 °C), reaching a maximum value at 1150 °C and then decreasing again at 1200 °C. The specimens sintered at 1350 °C showed anodic current densities very similar or close for different infiltration temperatures as shown in Figure 2b. When the specimens were sintered at 1450 °C (Figure 2c) the behaviour was different, i.e. the highest anodic current density was observed at the lowest infiltrating temperature, and its minimum value was at the intermediate infiltrating temperature. The E_{corr} value remained almost unaffected in all these cases.

The effect of ageing on the composites, either naturally or artificially, on the polarization curves is shown in Figure 3. These treatments had a slight negative effect on the anodic current density on the polarization curve of the Al-2024/TiC composite, but the passive region was retained. A slight increase, about 2 times, in the anodic current density is observed with these heat treatments. Although the $CuAl_2$ particles disappeared by dissolution in the aluminium under heat treatment [17], there are still other intermetallics such as Ti_3Cu, Al_3Ti, Ti_3AlC and Ti_3Al which are cathodic with respect to the metallic matrix.

The effect of the presence of binary Al–Cu_x alloy in the composite, on the polarization curve is shown in Figure 4a. This figure shows that for over-potentials lower than 250 mV, the anodic current density decreases

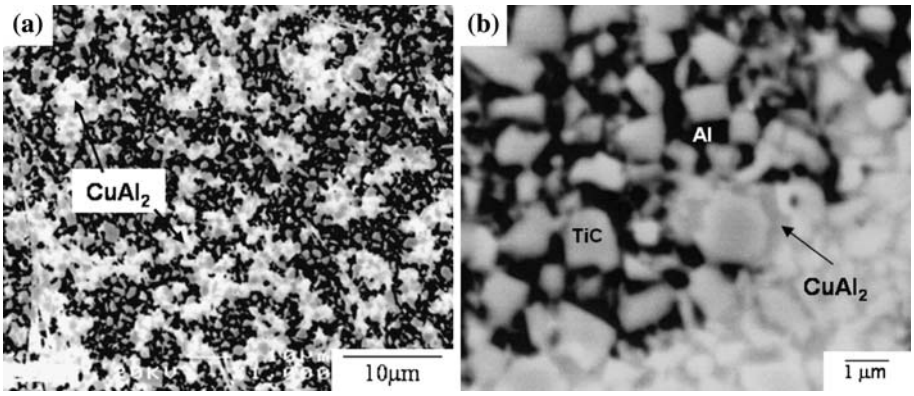

Fig. 1. Micrographs obtained by SEM of the composite sintered at 1250 °C and infiltrated at 1000 °C. (a) Al-20Cu/TiC and (b) Al-8Cu/TiC.

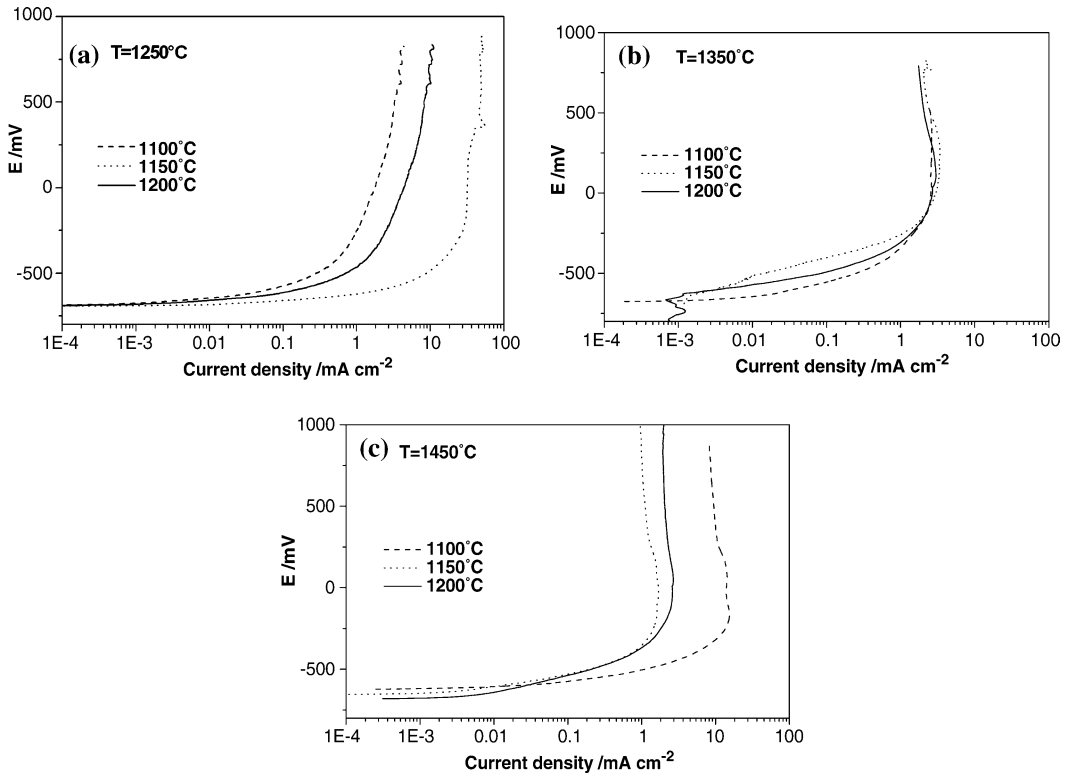

Fig. 2. Effect of the infiltration temperature on the anodic current density for Al-2024/TiC composites sintered at (a) 1250 °C, (b) 1350 °C and (c) 1450 °C.

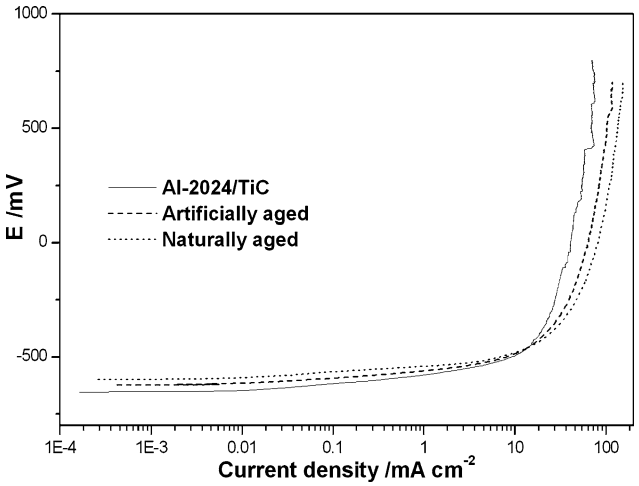

Fig. 3. Effect of heat treatment on the anodic current density for Al-2024/TiC composites.

with addition of Cu, and E_{corr} sometimes decreased but some other times increased. The opposite occurs at overpotentials higher than 250 mV, additions of Cu always increased the anodic current density. Similar behaviour is observed in the case of $AlMg_x$/TiC composites (Figure 4b). In all cases, increasing the Mg content in the composite increased the anodic current density values and decreased the E_{corr} values.

The effect of infiltrating temperature on the I_{corr} value for TiC performs sintered at 1250 °C is shown in Figure 5. In all cases the I_{corr} value of the TiC performs was lower than that for the Al-2024/TiC composite, except with the specimen infiltrated at 1100 °C after 15 h of exposure, which showed a higher I_{corr} value. The graph shows that, the I_{corr} value for the Al-2024/TiC composite remained stable with time; in contrast, the I_{corr} value for the TiC showed some instability due to the disruption of the protective layer.

Figures 6a and b, show the effect of additions of Cu or Mg on the corrosion current density as a function of time. As in the polarization curves, the addition of these elements always increased the I_{corr} values up to one order of magnitude, showing the detrimental effect of these elements. In most cases the I_{corr} values of the alloy without Cu or Mg remained stable during exposure, due to a stable protective Al_2O_3 or $Al(OH)_3$ layer.

Figure 7 shows the surface morphology of the Al-2024/TiC composite after immersion in 3.5 wt.% NaCl solution; a large number of pits are evident. The different sintering and infiltrating temperatures decreased the number of pits but they did not disappear completely, as shown in Figure 8, where localized corrosion is observed.

Figures 9 and 10 show that the addition of either Cu or Mg to the composites produce hollows and pits of larger diameter associated with localized attack of the protective Al_2O_3 or $Al(OH)_3$ layers by chloride ions [9–11]. The corrosion rate is accelerated by other factors such as the galvanic coupling of Cu^+ or Ti^+ containing particles in the Al-matrix. The nucleation of the pit occurs in the TiC-matrix and intermetallic compound-matrix interfaces. These sites act as discontinuities where the protective film can easily be disrupted. Similar results were found by Kiourtsidis et al. [19] who studied the corrosion behaviour of the squeeze-casting aluminium alloy 2024, reinforced with SiC particulate, in 3.5 NaCl. No detrimental galvanic effect was observed between the reinforcement phase and the matrix; instead, corrosion was described by the dissolution of the α-phase adjacent to the $CuAl_2$ interdendritic regions and pitting corrosion of the more cathodic phase, in this case, the dendrite cores. Additionally, Wrinkler et al. [20], by incorporating latex fibers into 7XXX aluminium alloys, observed pitting corrosion, preferentially at the grain boundaries and fiber/matrix interface regions, when the alloys were corroded in 3.5 NaCl solutions. Rapid dissolution occured inside the pitting, while there is an existing oxygen reduction process taking place on the adjacent surfaces. There is a high concentration of Al^{3+} ions inside the pits as a result of the cationic hydrolysis and there is an increase in hydrogen ions, according to the following reaction:

$$Al^{3+} + 3H_2O \rightarrow Al(OH)_3 + 3H^+ \quad (2)$$

This process reduces the pH inside the pit and material transfer to the adjacent zone, occurs by ion

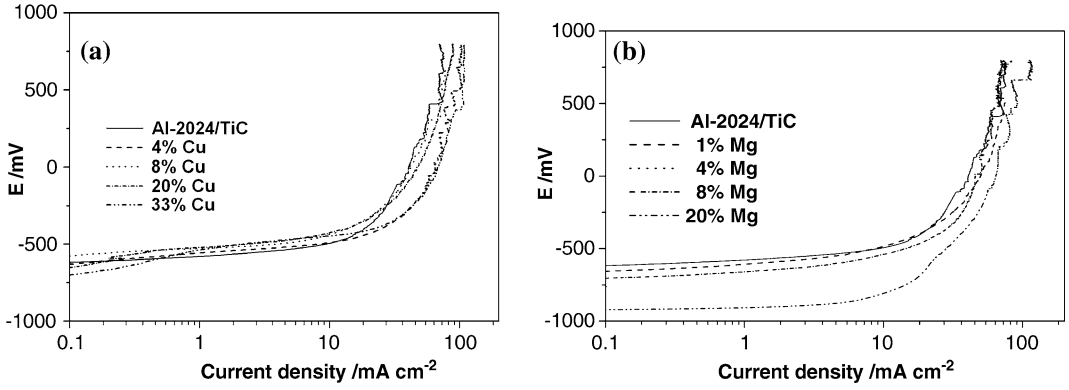

Fig. 4. (a) Effect of Cu and (b) Mg additions on anodic dissolution of the $AlCu_x$/TiC and $AlMg_x$/TiC composites.

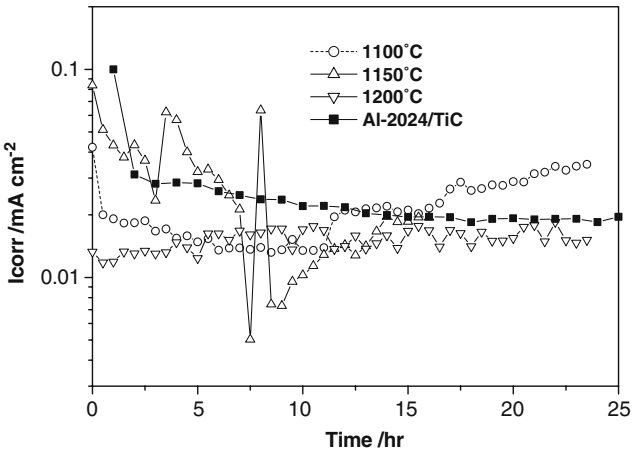

Fig. 5. Effect of the infiltration temperature on I_{corr} as a function of the time on Al-2024/TiC composites sintered at 1250 °C.

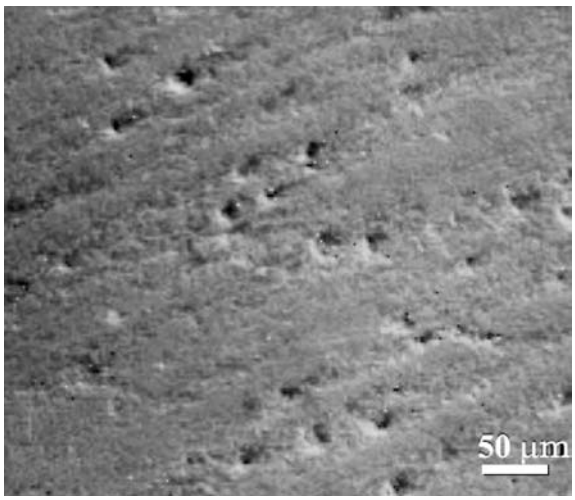

Fig. 7. Micrograph obtained by SEM of Al-2024/TiC composite corroded in 3.5% NaCl, where some pits can be observed.

transport in the electrolyte [21]. Intermetallic Cu–Al compounds are strongly cathodic inside the matrix and act as cathodic sites, facilitating the disruption of either Al_2O_3 or $Al(OH)_3$ protective layers and enhancing pitting corrosion. When second phases are present, such as Cu^- or Ti^- rich particles, they act as effective cathodes, leading to the formation of micro-galvanic cells, enhancing the anodic dissolution of the metallic matrix in the form of pits.

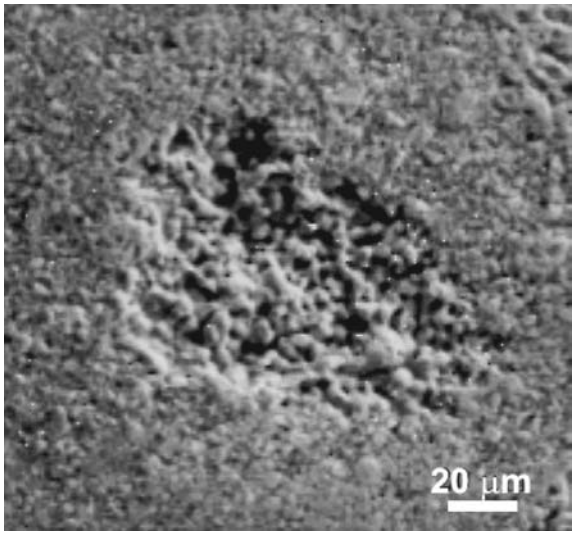

Fig. 8. Micrograph obtained by SEM of Al-2024/TiC composite sintered at 1450 °C and infiltrated at 1200 °C corroded in 3.5% NaCl.

4. Conclusions

From the studies carried out in this work, on Al-2024/TiC, $AlCu_x$/TiC and $AlMg_x$/TiC composites produced by the pressureless infiltration technique the following conclusions may be drawn:

1. In the case of the Al-2024/TiC composites, the anodic current density was reduced, decreasing the amount and size of the pits. This was independent of the sintering and infiltrating temperatures.
2. For composites, either artificially or naturally aged, the anodic corrosion current density increases and the number and depth of pits decrease.
3. There is no direct relationship between the anodic current density and the sintering or infiltrating temperatures.

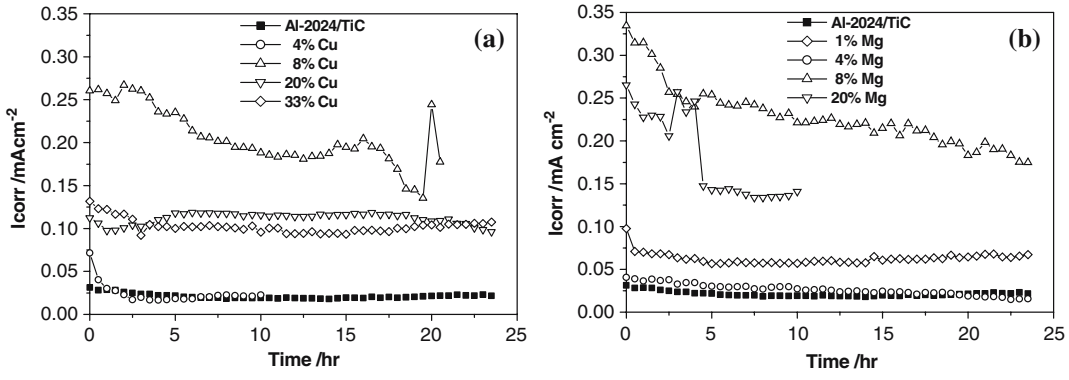

Fig. 6. (a) Additions effect of Cu and (b) Mg on I_{corr} vs time obtained of the Al-Cu_x/TiC and $AlMg_x$/TiC composites.

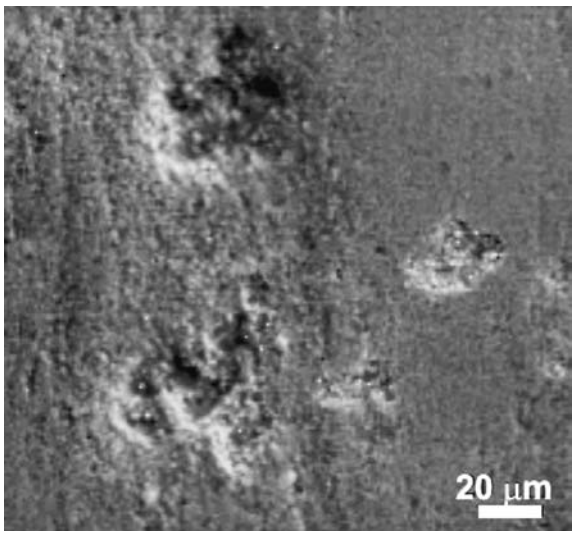

Fig. 9. Micrograph obtained by SEM of Al-4Mg/TiC composite corroded in 3.5% NaCl solution.

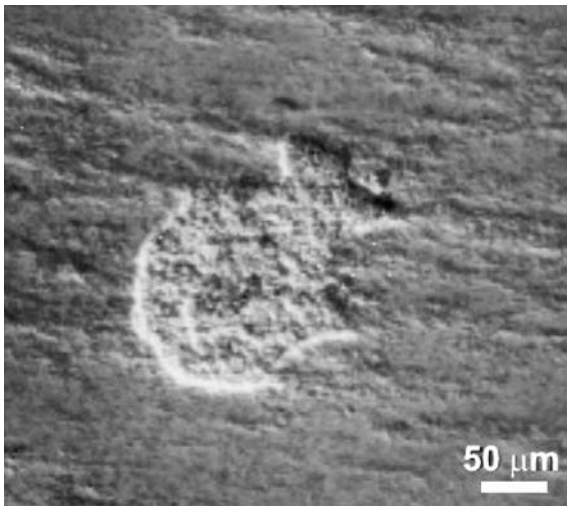

Fig. 10. Micrograph obtained by SEM of Al-20Cu/TiC composite exposed in 3.5% NaCl solution showing a localized corrosion.

4. The galvanic effect of Cu and Ti-rich particles to the Al-alloy enhances pitting corrosion.
5. The anodic current density increases with the addition of either Cu or Mg. However, the pits are shallower and larger in diameter than those found in the Al-2024/TiC composite.

References

1. C.A. León, V.H. López, E. Bedolla and R.A.L. Drew, *J. Mater. Sci.* **37** (2002) 3509.
2. A. Contreras, C.A. León, R.A.L. Drew and E. Bedolla, *Scripta Mater.* **48** (2003) 1625.
3. D. Muscat, K. Shanker and R.A.L. Drew, *Mater. Sci. Technol.* **8** (1992) 971.
4. A. Contreras, A. Albiter and R. Pérez, *J. Phys: Condensed Matter* **16** (2004) S2241.
5. A. Contreras, E. Bedolla and R. Pérez, *Acta Mater.* **52** (2004) 985.
6. R.L. Deuis, L. Green, C. Subramanian and J.M. Yellup, *Corrosion* **53**(11) (1997) 880.
7. D. Nath and T.K.G. Namboodhirt, *Corrosion Sci.* **29**(10) (1989) 1215.
8. P.C.R. Nunes and L.V. Ramanathan, *Corrosion* **51**(8) (1995) 610.
9. Y. Shimizu, T. Nishimura and I. Matsushima, *Mat. Sci. Eng.* **A198** (1995) 113.
10. H.Y. Yao and R.Z. Zhu, *Corrosion* **54**(7) (1998) 499.
11. R.C. Paciej and V.S. Agarwala, *Corrosion* **44**(10) (1988) 680.
12. H. Sun, E.Y. Koo and H.G. Wheat, *Corrosion* **47**(10) (1991) 741.
13. P. Trzaskoma, *Corrosion* **46** (1990) 402.
14. L.H. Hihara and R.M. Latanision, *Corrosion* **48** (1992) 546.
15. O.P. Modi, M. Saxena, B.K. Prasad, A.H. Yegneswaran and M.L. Vaidya, *J. Mater. Sci.* **27** (1992) 3897.
16. M. Stearn and A.L. Geary, *J. Electrochem. Soc.* **105** (1958) 638.
17. A. Albiter, A. Contreras, E. Bedolla and R. Perez, *Composites* **34A** (2003) 17.
18. A. Contreras, V.H. López and E. Bedolla, *Scripta Mater.* **51** (2004) 249.
19. G. Kiourtsidis and M. Skolianos, *Mat. Sci. Eng.* **A248** (1998) 165.
20. S.L. Wrinkler, M.P. Ryan and H.M. Flower, *Corrosion Sci.* **46** (2004) 893.
21. Marcel Pourbaix, Atlas of electrochemical equilibria in aqueous solutions, NACE, Houston Tx, USA CEBELCOR, pp. 168.